IRAQI Academic Scientific Journals
Samarra Journal of Pure and Applied Science
SJPAS
www.sjpas.com
p ISSN: 2663-7405
e ISSN: 2789-6838

Study on the Structural and Optical Properties of CuO Thin Films Mixed with La_2O_3 Deposited using Pulsed Laser Deposition for Future Optoelectronic and Gas Sensing Devices Applications

Abeer M. Enad and Jamal M. Rzaij*
Department of Physics, College of Science, University Of Anbar, Ramadi, Iraq

https://doi.org/10.54153/sjpas.2025.v7i2.1123

Article Information
Received: 15/01/2025
Revised: 13/02/2025
Accepted: 20/03/2025
Published: 30/06/2025

Keywords:
Copper oxide, Rare earth elements, PLD, La_2O_3, Optoelectronics, Gas sensor .

Corresponding Author
Mobile:
E-mail:
sc.jam72al@uoanar.edu.iq

Abstract

The mix of thin metal oxide coatings with rare earth elements demonstrates great potential for improving structural and optical properties in advancing optoelectronic devices and gas sensors. This study investigated the impact of varying weight ratios mixing of lanthanum oxide (La_2O_3) on copper oxide (CuO) thin films' structural, topographic, microstructural, and electronic transition characteristics. The characteristics of films developed via pulsed laser deposition were examined utilizing X-ray diffraction (XRD), energy-dispersive X-ray (EDX) spectroscopy and atomic force microscopy (AFM), field emission scanning electron microscopy (FE-SEM), photoluminescence (PL) and UV-Vis spectroscopy analysis. According to the structural analysis, the polycrystalline copper oxide film crystallized with a dominating peak towards the (111) diffraction peak. The dominant peak intensity decreased as the lanthanum oxide content increased, and the crystal size reduced from 19 to 17.4 nm. The elemental analysis confirmed the presence of O, Cu, and La elements and no other EDX emission peaks corresponding to additional elements or impurities. The as-deposited CuO film had a wide nano-grain distribution, with an average grain size of 100 nm and an average RMS of 3.7 nm. In contrast, the La_2O_3 mixed-CuO samples showed a decrease in average grain size and increased RMS to 4.9 nm for the largest La_2O_3 mixing ratio. The optical analysis verified a reduction in the CuO absorbance spectrum and a blue shift in the absorption edge with an increasing mixing ratio of La_2O_3, raising the optical energy gap from 2.25 eV to 2.85 eV. The results indicate that the mixing of La_2O_3 substantially modifies the structural and optical characteristics of CuO thin films, rendering the developed films suitable candidates for gas sensing and optoelectronic applications.

Introduction

Due to their appealing features, copper oxides have been widely studied in semiconductor physics. The copper oxide family includes two stable oxides: cuprous oxide (Cu_2O) and cupric oxide (CuO) [1]. These oxides exhibit distinct physical, chemical, and optical characteristics. Notably, CuO thin films are p-type semiconductors with an optical bandgap of approximately 2.6 eV [2]. Several techniques have been employed for depositing CuO thin films, each offering

unique advantages and suitability for specific applications. Various deposition techniques, including sputtering [3], thermal evaporation [4], oxidation [5], molecular beam epitaxy [6], and electrodeposition [7], have been used to fabricate CuO films.

Among these techniques, pulsed laser deposition (PLD) is a highly effective method for thin film fabrication, particularly in preserving stoichiometry in complex material. PLD involves using a high-energy pulsed laser to ablate a target material in a vacuum chamber, generating a plasma plume that subsequently deposits onto a substrate. This method allows precise control over film thickness, composition, and crystallinity. Although PLD is not widely utilized for CuO deposition, it has demonstrated the capability to produce thin film with enhanced structural and optical characteristics [8]. CuO is widely used in various applications owing to its availability of constituent elements in nature, thermal stability, and outstanding electrochemical characteristics. CuO thin films are attractive materials for optical applications [9, 10], energy storage devices [11], a saturable absorber layer [12], and gas sensors [13] owing to their semiconducting characteristics.

Rare earth elements (REE) are valuable resources owing to the unique electrical, optical, and chemical properties of their 4f-shell ions. They are widely used in magnets, catalysts, high-performance luminescence devices, and other materials [14]. The rare earth element La2O3 is commonly used in thermoluminescence, luminescence, supercapacitor applications, and photonics [15]. CuO is categorized as a p-type semiconductor, indicating that the predominant charge carriers in the material are holes [16]. Likewise, La_2O_3 is classified as a p-type semiconductor, indicating that holes are the primary charge carriers. When layers of CuO and La_2O_3 are combined to form a heterojunction, the surface of CuO-La_2O_3 heterostructures enables effective charge-transfer processes. The difference in work function between La_2O_3 (2.3 eV) and CuO (5.32 eV) leads to electron transfer from La_2O_3 to CuO, resulting in the formation of heterojunctions until the Fermi levels are balanced, thereby modifying the electrical properties of CuO- La_2O_3 heterostructures [15, 17]. This study aimed to prepare nanostructured copper oxide thin films incorporated with various ratios of La_2O_3 using the one-step PLD technique. This project investigates the impact of incorporating La_2O_3 into CuO thin films on their structural and optical characteristics, representing a notable advancement in creating innovative materials that enhance the functionality of semiconductors for future gas sensing applications.

Materials and Purity

High-purity materials were used in this work to ensure reliable and reproducible results. Copper oxide (CuO) powder with 99.999% purity(from Aldrich) and lanthanum oxide (La_2O_3) powder with 99.999% purity (from Sigma-Aldrich) were employed to fabricate CuO-La_2O_3 composite thin films. La_2O_3 was added to CuO at weight ratios of 1 wt.%, 3 wt. %, and 5 wt. %, labeled as L1, L3, and L5, respectively. All chemicals were used in their raw form to maintain consistency across the experiment.

Experimental work

A pulsed laser deposition (PLD) technique was employed at room temperature (28°C) to deposit CuO and La_2O_3-mixed CuO thin films on silicon substrates. The laser wavelength was 1064 nm, with a pulse energy of 200 mJ and a repetition frequency of 6 Hz. The deposition chamber was equipped with a substrate mask and a rotating target holder, as shown in Fig.1. Thin film deposition was conducted in the vacuumed chamber. The target-substrate distance was adjusted to 2 cm, and the laser gun-target distance was adjusted to 5 cm. A CuO thin film

was developed by compressing 5 grams of CuO powder with a purity of 99.999% (by Aldrich) into a pellet target 2 cm in diameter and 0.5 cm in thickness by applying a 15-ton hydraulic press for 24 hours. The film deposition was conducted under a vacuum of 2.2×10^{-2} kPa. The La_2O_3-incorporate CuO films were prepared by repeating the previous procedure by adding La_2O_3 powder at weight ratios of 1 wt.%, 3 wt.%, and 5 wt.% to the CuO powder, which were denoted to as L1, L3, and L5, respectively. Thin film thickness is determined by analyzing the cross-sectional FE-SEM images with the assistance of ImageJ software.

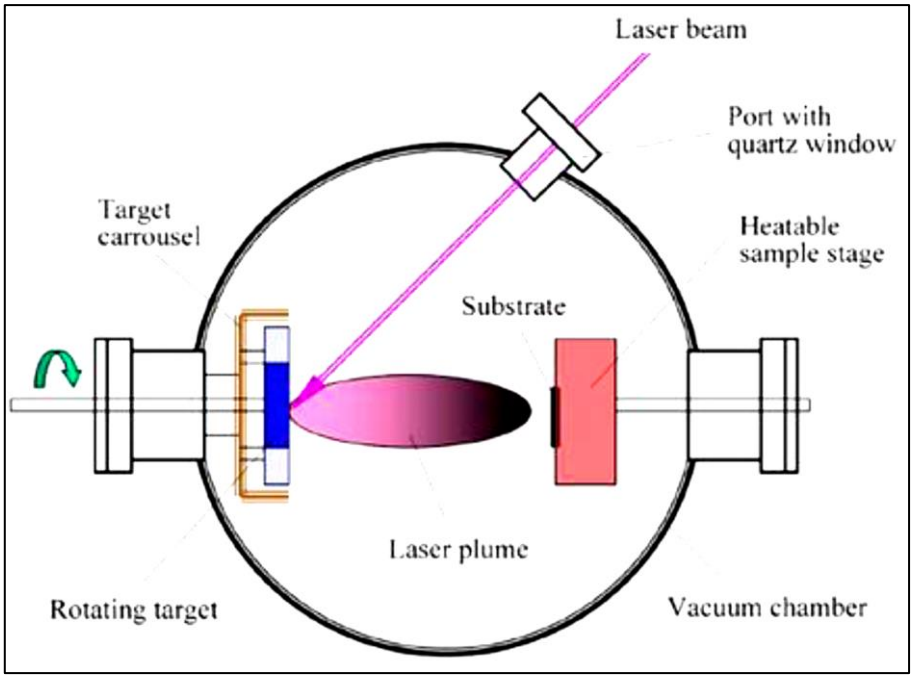

Fig.1 Schematic diagram of a typical laser deposition set-up.

Results and discussion

X-ray diffraction (XRD) investigation:

Fig.2 shows the XRD patterns of CuO and CuO mixed with La_2O_3 thin films displayed in thin films deposited on a silicon substrate. The intense peak at a diffraction angle of $2\theta\approx69°$ corresponds to the (111) direction of the Si substrate. Four distinguished XRD diffraction peaks were observed for the as-deposited CuO thin film corresponding to (10-1), (111), (20-2), and (-113) of monoclinic CuO structure according to JCPDS card No. 96-101-1195. Scherrer's formula (Equation (1)) was utilized to determine the crystallite size (D) [18], which was found to be 19 nm. The X-ray diffraction pattern did not show any additional phase, which refers to the purity of prepared films.

An additional peak appeared at 29.7° for a high La-mixing ratio, corresponding to the (101) plane of the La_2O_3 structure JCPDS NO 05-0602. The intensity of these peaks increased with an increasing mixing ratio. The increase in peak intensity is due to improved crystallinity, higher La_2O_3 phase concentration, reduced lattice strain, and the stronger X-ray scattering power of La atoms enhancing diffraction signals.

$$D = \frac{(0.9\times\lambda)}{(\beta\times Cos(\Theta)} \qquad (1)$$

where θ is the diffraction angle, λ is the wavelength of XRD spectra, and β is the full width at half maximum (FWHM) of the peaks. Table 1 lists the XRD parameters of the analyzed samples. The average crystallite size was reduced from 19 nm for the as-deposited samples to 17.4 nm for the L5 sample. The decrease in crystallite size may be due to the difference in the atomic radius of the host matrix and the mixed material. The crystal structure in the La_2O_3-mixed CuO film remains unchanged except for a slight change in the peak positions. The diffraction peak shift was attributed to the induced lattice strain caused by the lanthanum mixing, which can be associated with the different sizes of copper and lanthanum atomic radius [19].

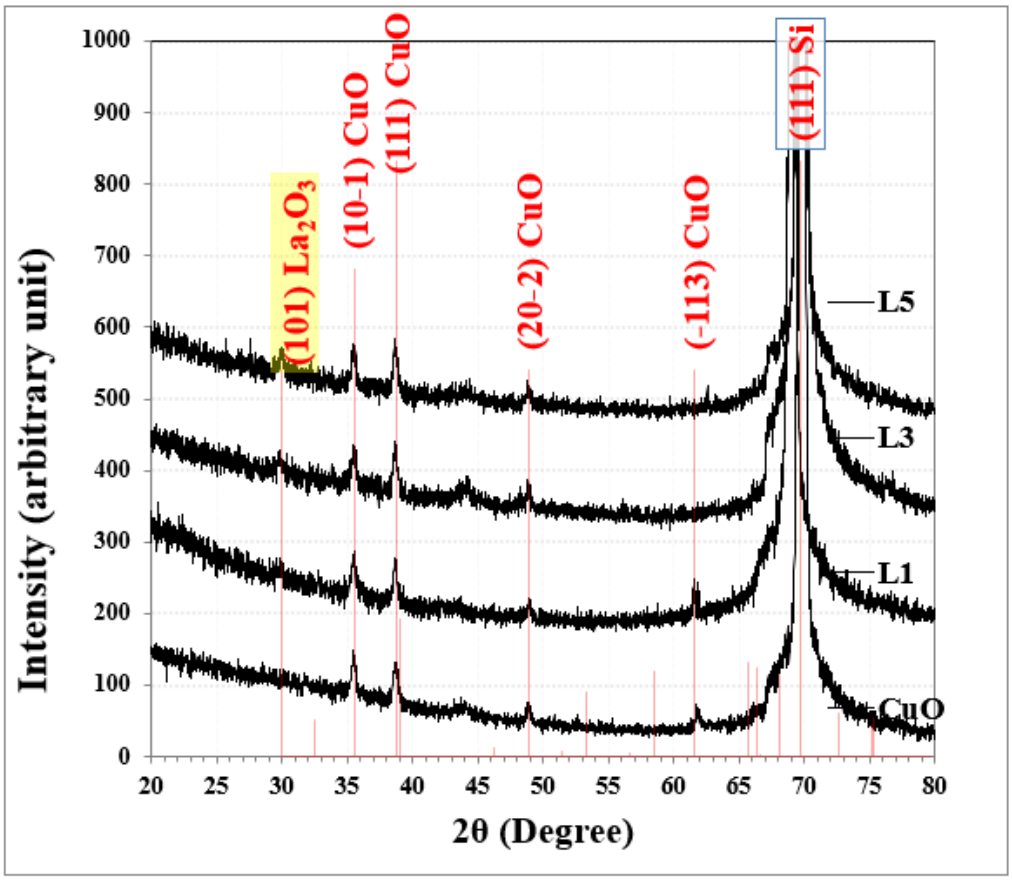

Fig.2 XRD spectra of the as-deposited and La_2O_3-mixed CuO thin films at various ratios

Table 1: XRD parameters of pure and La_2O_3-mixed CuO thin films prepared at different ratios.

Sample	2θ (Deg.)	FWHM (Deg.)	d_{hkl} Exp.(Å)	hkl	Phase	D (nm)	Average D (nm)
As-deposited CuO	35.5353	0.3779	2.5243	(10-1)	CuO	22.1	19
	38.7264	0.5038	2.3233	(-111)	CuO	16.7	
	48.8873	0.4619	1.8615	(20-2)	CuO	18.9	
	61.8195	0.5039	1.4996	(-113)	CuO	18.4	
L1	35.5239	0.4204	2.5251	(10-1)	CuO	19.9	18.3
	38.6934	0.4528	2.3252	(-111)	CuO	18.6	
	48.9133	0.6145	1.8606	(20-2)	CuO	14.2	
	61.5589	0.4528	1.5053	(-113)	CuO	20.4	
L3	29.7671	0.4204	2.999	(-101)	La_2O_3	19.6	17.9
	35.5563	0.5174	2.5228	(10-1)	CuO	16.1	

	38.7257	0.4705	2.3233	(-111)	CuO	17.9	
	48.881	0.4828	1.8618	(20-2)	CuO	18.1	
L5	29.9935	0.5175	2.9768	(-101)	La_2O_3	15.9	17.4
	35.4916	0.4528	2.5273	(10-1)	CuO	18.4	
	38.6934	0.4851	2.3252	(-111)	CuO	17.4	
	48.9133	0.4851	1.8606	(20-2)	CuO	18	

Energy-dispersive X-ray (EDX) analysis

Fig.3 shows the EDX spectra of the CuO and CuO thin films mixed with various La_2O_3 contents.

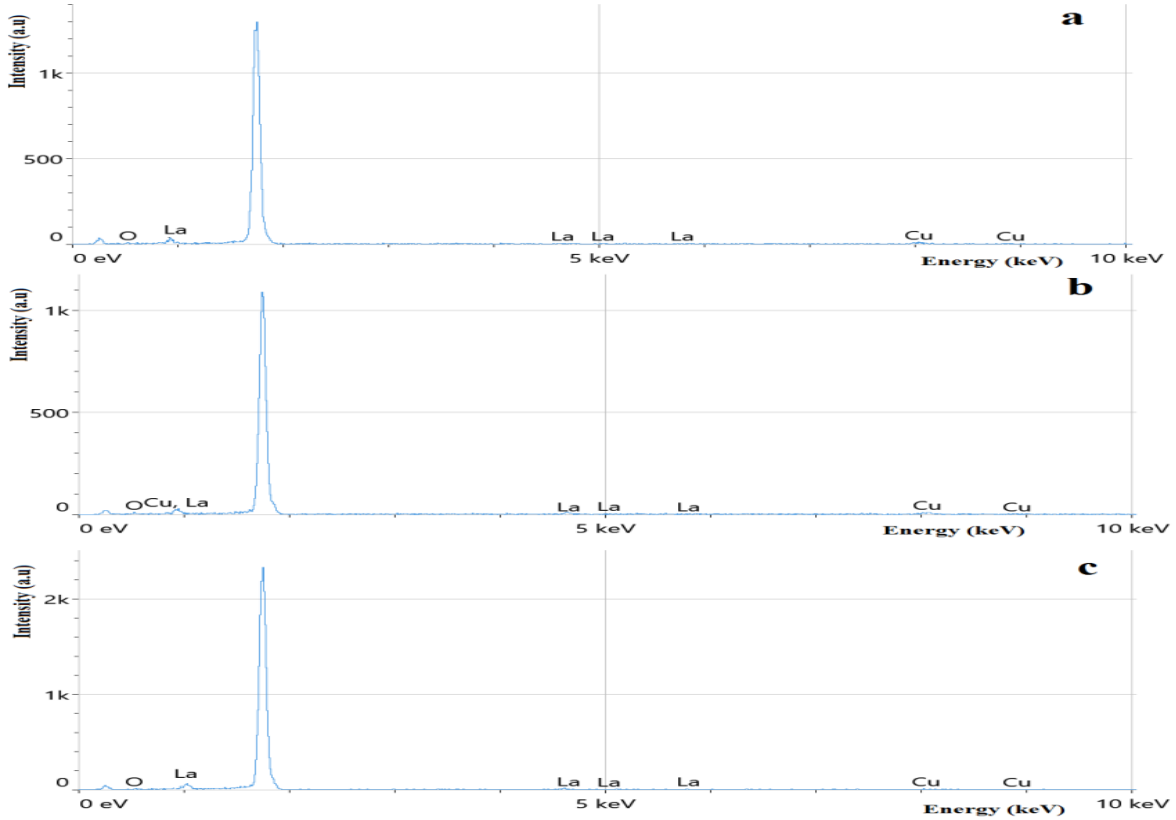

Fig.3 EDX spectra of La_2O_3 –mixed CuO thin films at different mixing ratios (a) 1%, (b) 3%, and (c) 5%

The elemental analysis confirmed the presence of O, Cu, and La elements and no other EDX emission peaks corresponding to additional elements or impurities. The analysis confirmed a decline in the copper-weighted ratios (Cu wt%) with a rise in the lanthanum oxide mixing ratio, indicating that the lanthanum was effectively mixed in the copper matrix. The high-intensity peak at 1.7 keV corresponds to the Si substrate. Table 2 lists the elemental analysis results of the CuO and La_2O_3-mixed CuO thin film at various mixing ratios.

Table 2: EDX analysis of the La_2O_3 –mixed CuO thin film at different mixing ratios

Atomic %	Wt.%

Element	O	Cu	La	O	Cu	La
L1	63.6	35.1	1.3	29.7	65.1	5.1
L3	66.4	31.8	1.8	31.9	60.6	7.6
L5	80.1	16	3.9	45.1	35.8	19.1

Topographical analysis

Fig.4(a-d) shows the topographical 3D test Atomic Force Microscopy (AFM) images of the prepared thin films. Root mean square (RMS) analysis was adopted to evaluate the surface roughness of the deposited films, which statistically is the deviation in the deposited atoms' height from the film surface's mean level.

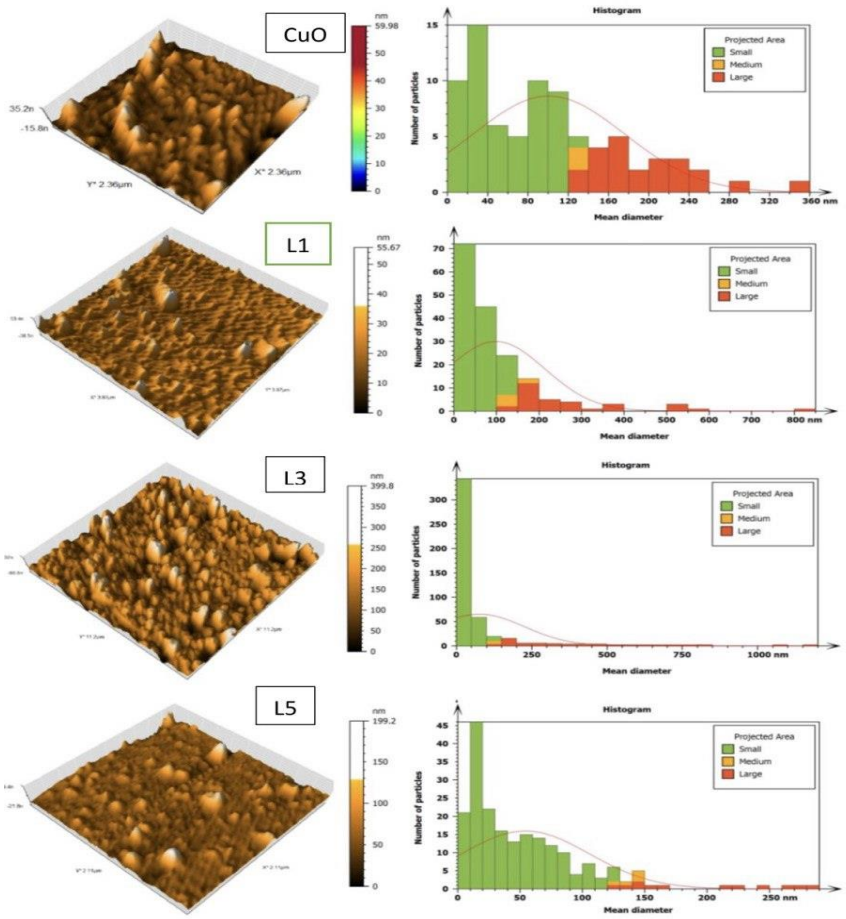

Fig.4 AFM images of the CuO and La_2O_3-mixed CuO thin films at different ratios

The as-deposited CuO sample (Fig.4a) revealed a wide nano-grain size distribution with an average 100 nm and an average RMS of 3.7 nm. The mixed sample with 1 wt.% and 3 wt.% La_2O_3 (Fig. 4b and C) decreased the average grain size to 98 nm and 76 nm with an enhancement in the RMS to 4.4 nm and 4.9 nm, respectively. The decrease in grain size is due to La_2O_3 inhibiting grain growth by pinning grain boundaries and introducing structural distortions. La_2O_3 alters the surface energy and promotes smaller, stabilized grains, enhancing surface roughness and material uniformity [20]. When the La_2O_3 increased to 7 wt.%, the topographical RMS decreased to 4 nm. The average grain size decreased to 54 nm with a more

homogeneous atomic distribution, as shown in Fig.4c. The surface roughness and smaller particle size offer a large surface area, effective more gas molecule adsorption, influencing the performance of gas sensor devices [21, 22].

Table 3: Average diameter and RMS of the As-deposited CuO La_2O_3-mixed CuO thin films at different ratios

Sample	Average Diameter (nm)	Roughness (nm)	RMS roughness (nm)
As-deposited CuO	100.8	26.58	3.7
L1	98.56	46.19	4.4
L3	76.56	26.46	4.9
L5	54.3	13.06	4

Surface morphology investigations:

Fig.5 presents the Field emission scanning electron microscopy (FE-SEM) of the pure and La_2O_3 mixed CuO thin films fabricated under varying La_2O_3 mixing ratios.

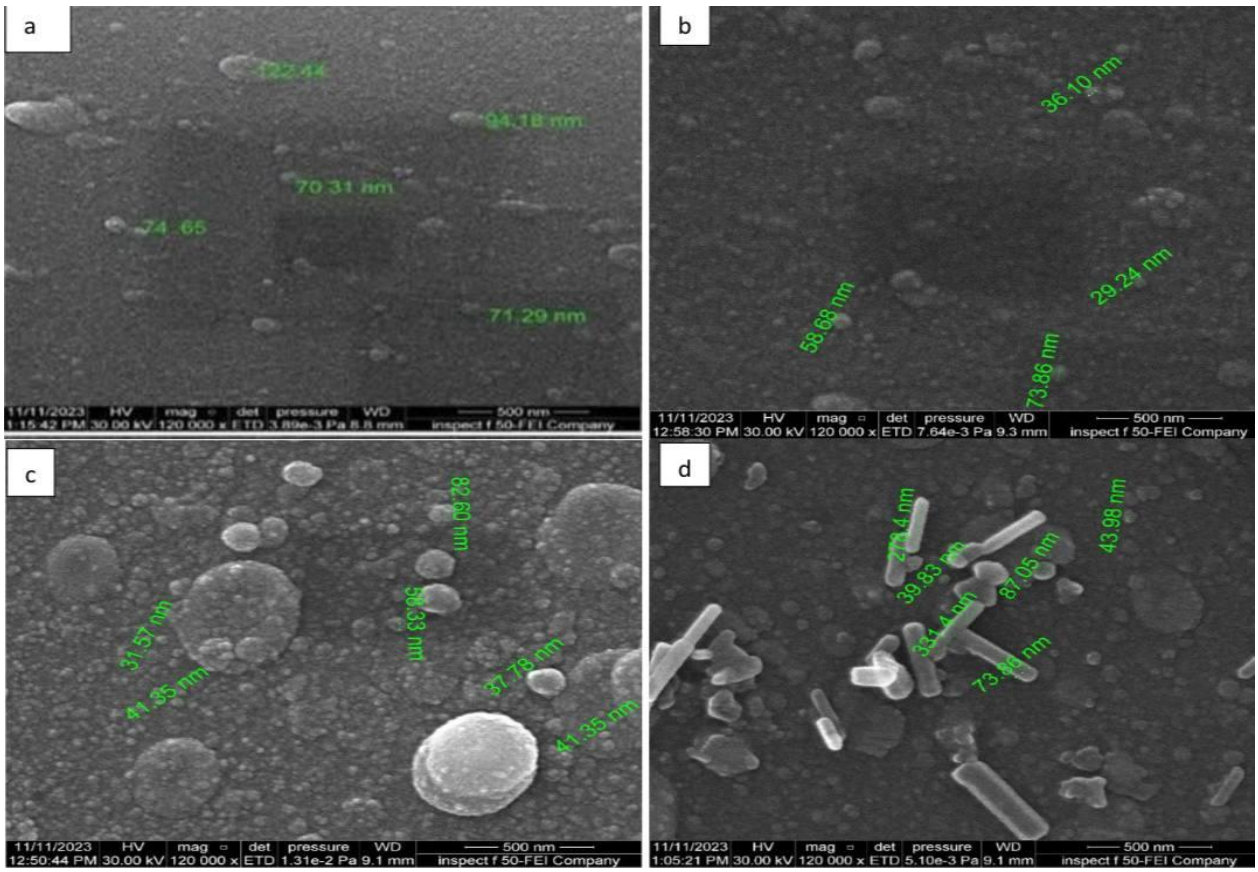

Fig.5. Top view FE-SEM images (a) CuO, (b), L1 (c), L3, and (d) L5- samples

The findings illustrate a smooth surface for the as-deposited sample, interspersed with nanostructural particles ranging in size from 70 to 94 nm. Adding La_2O_3 to CuO thin films alters their surface morphology. Initially, smooth films develop nanostructures as La_2O_3 concentration increases. This suggests La_2O_3 disrupts CuO film growth, leading to a rougher surface with increased nanoparticle density. The smooth surface of the as-deposited sample was gradually composed of nanostructures attached to the sample surface as the La content increased. Semi-spherical nanoparticles with average nanoparticle diameters ranging from

about 29 to 73 nm for the L1 sample and increasing the La content to 3% caused an increase in the diameter of attached spheres to reach around 500 nm. The increase of the La2O3 mixin ratio to 5wt.% resulted in a variation in the nanostructure to rod-like structures attached to the sample surface with diameters of about 70 nm and lengths of 330 nm. These rod-like nanostructures suggested separate phases of La_2O_3, confirmed by the XRD results at high La_2O_3 ratios. The same La_2O_3 structure was prepared under specific conditions, as described in a previous study [23]. The cross-sectional images of the La_2O_3 mixed thin film prepared at different mixing ratios on Si substrates (Fig. 5e-g) show a well-stacked thin film on the substrates without any defects or cracks, indicating the compatibility between the deposited films and the substrates.

Photoluminescence (PL) results

Fig. 6 shows the PL spectra of the CuO pure and La_2O_3-mixed CuO thin films, with varying percentages compared with the pure CuO pattern in the wavelength range 500–1200 nm at room temperature.

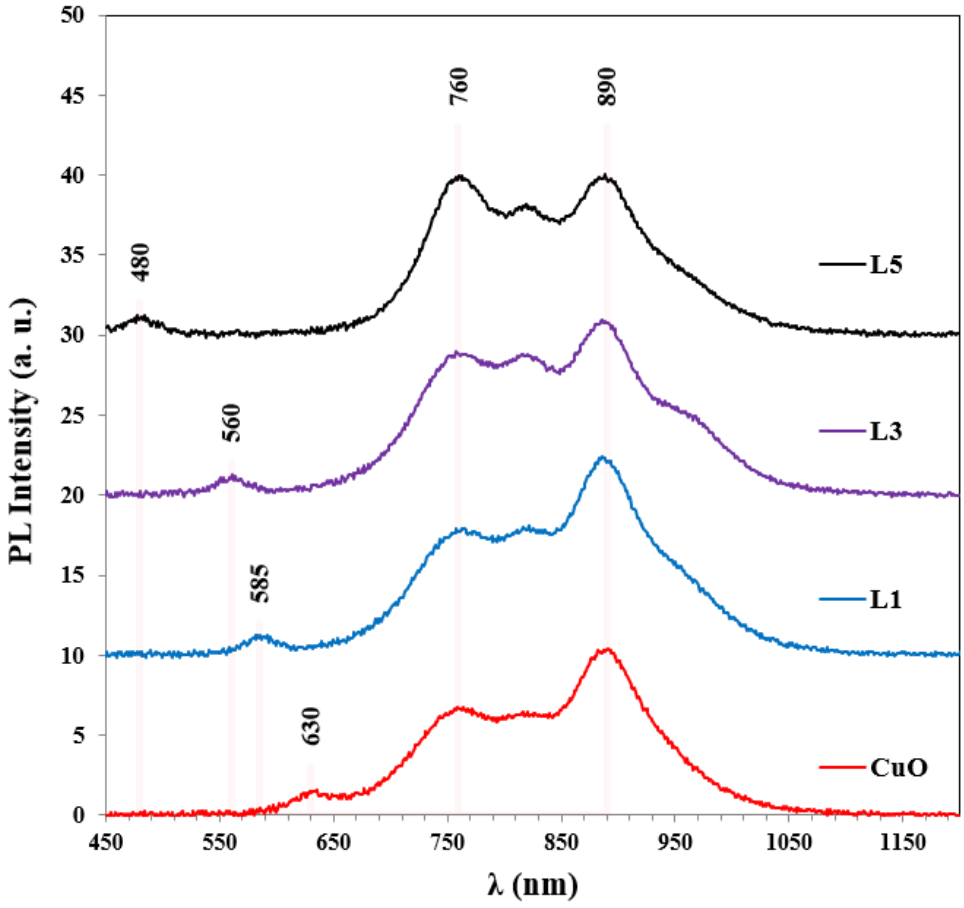

Fig.6 PL spectra of the CuO and La_2O_3 mixed with CuO thin films at various mixing ratios

Three distinct peaks were observed in all samples. A broadband peak at approximately 630 nm (1.97 eV) is attributed to the band-to-band transition of CuO facilitated by phonon-assisted emission. The peaks centered around 760 nm (1.63 eV) and 890 nm (1.39 eV) are likely associated with oxygen vacancy and copper vacancy, respectively, owing to electronic transitions between oxygen interstitials and copper vacancies [24].

The PL spectra of the mixed samples with La_2O_3 exhibited a blue shift, suggesting a change in the material's electronic structure due to the incorporation of La_2O_3 in emission related to the band-to-band transition, specifically at 585 nm (2.12 eV), 560 nm (2.21 eV), and 480 nm (2.58 eV) for the L1, L3, and L5 samples, respectively. The two peaks corresponding to oxygen and copper vacancies were fixed at the same positions but at different intensities. Minor peaks at approximately 820 nm can be attributed to non-stoichiometric defect-assisted recombination [25]. The increasing intensity of the photoluminescence band at 760 nm indicates an increase in the number of oxygen vacancy defects. Increasing the band intensity at 760 nm while reducing the band intensity at 890 nm with increasing the L_2O_3 content indicated an increase in the oxygen vacancies while reducing the metal vacancies. Oxygen vacancies play a crucial role in the gas-sensing mechanism of La-mixed CuO thin films. For gas sensing devices, the oxygen vacancies modified the electronic structure, increasing the interaction between gas molecules and the electrons trapped at these oxygen vacancies at the material's surface, leading to large variations in electrical conductivity.

UV-visible spectroscopy analysis

The optical absorption spectra of the as-deposited CuO and CuO mixed with La_2O_3 thin films are shown in Fig.7. A decrease in absorbance and a blue shift in the absorption edge were observed with increasing the mixing ratio of La_2O_3. The incorporation of La_2O_3 causes changes in the band structure, increasing the optical bandgap. Increasing the La_2O_3 mixing ratio caused the absorption edge to shift toward shorter wavelengths (blue shift). This behavior is typically associated with quantum confinement effects or changes in the crystal structure, which alter the material's electronic properties. The La_2O_3 mixing may introduce defects such as oxygen vacancies into the CuO crystal lattice. These defects can modify the electronic structure by introducing localized states within the band gap, affecting absorption behavior [26]. This property is effective for solar cells and optoelectronic devices.

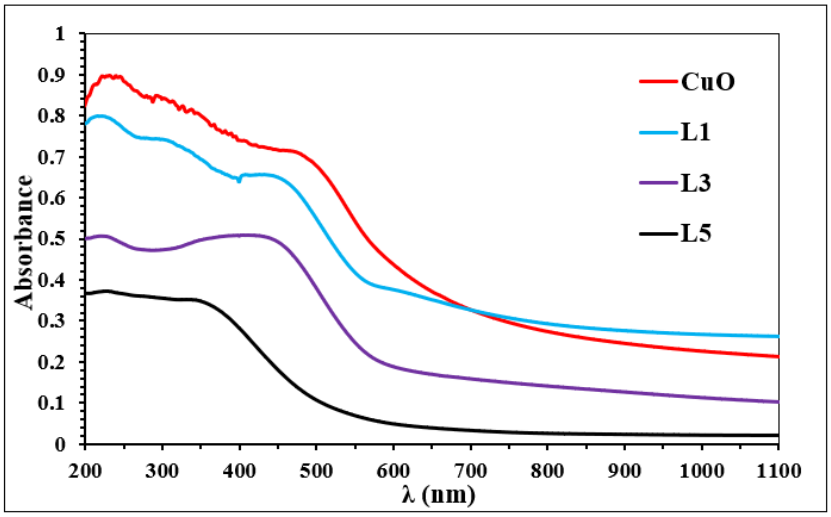

Fig.7 UV-vis spectra of the as-deposited and La_2O_3 mixed-CuO thin films

The Tauc plot determined the direct and indirect optical energy band gaps (Eg) in pure and La-mixed CuO thin films. The Eg is obtained from the intercept point of the tangential line with the X-axis [27], as illustrated in Fig.8.

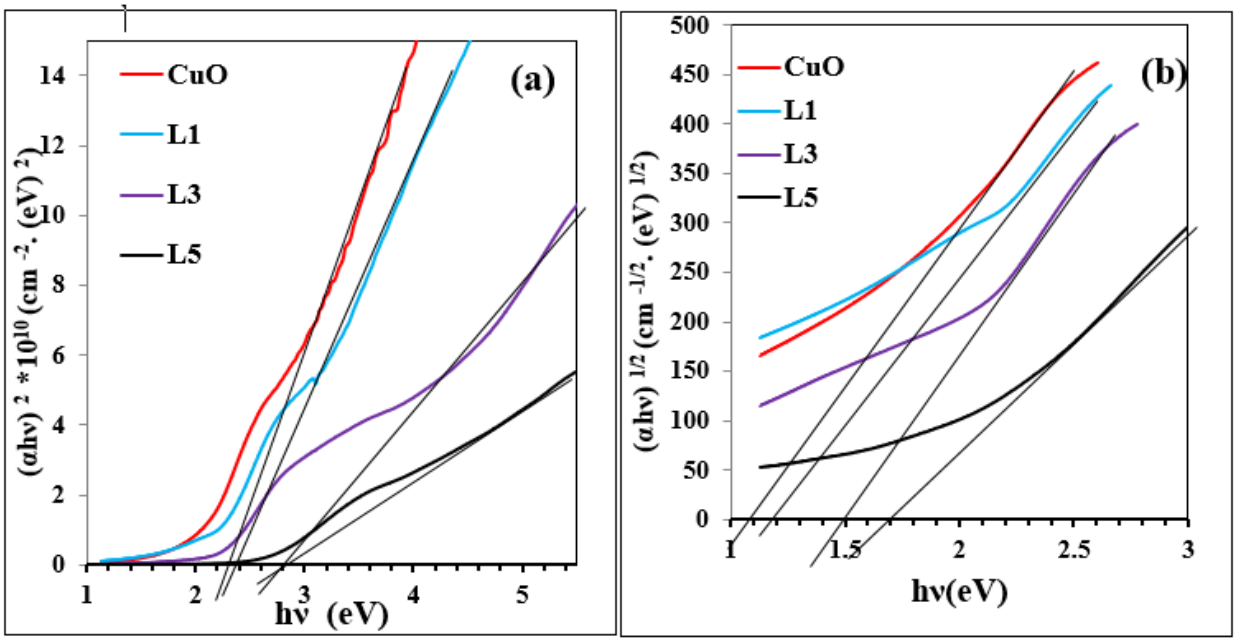

Fig.8 Tauc plot of the as-deposited and La_2O_3 mixed-CuO thin films (a) direct and (b) indirect transitions

Table 0: Direct and indirect E_g values for each sample

Samples	Direct Eg (eV)	Indirect Eg (eV)
CuO	2.25	1.1
L1	2.4	1.2
L3	2.8	1.5
L5	2.85	1.7

The outcomes validate an increase in direct and indirect band gaps with increasing the La_2O_3 concentrations, from 2 to 2.3 eV and from 1.1 to 1.7 eV for direct and indirect transitions, respectively, as demonstrated in Table (4). This increase in the energy bandgap is attributed to a reduction in the crystalline size, as evidenced by the XRD results [28]. In addition, an increasing bandgap appeared in degenerately mixed semiconductors, where the carrier concentration was sufficiently high for the Fermi level to approach the bottom or top of the conduction or valence band [29].

Conclusions

In this work, the as-deposited and La_2O_3 mixed-CuO thin films have been successfully deposited using pulsed laser deposition. La_2O_3 incorporation leads to detailed changes in structural characteristics, morphological features, and optical properties of CuO thin films deposited by pulsed laser deposition (PLD). The results show that mixing La_2O_3 with CuO leads to modifications of crystallite dimensions and the film surface characteristics. The promising nature of rare-earth mixing for enhancing CuO-based material properties becomes evident when considering decreased grain size alongside raised surface roughness and transformed electronic band structure. Oxygen vacancies within the films are essential in changing PL spectrum and bandgap widths, resulting in higher carrier mobility and better gas adsorption performance. The findings of La_2O_3-mixed CuO thin films indicate their potential to

be attractive determinations for optoelectronic devices and environmental sensing applications.

References

1. Rzaij, J. M., & Habubi, N. F. (2022). Enhancing the CO2 sensor response of nickel oxide-doped tin dioxide thin films synthesized by SILAR method. Journal of Materials Science: Materials in Electronics, 33(15), 11851–11863. https://doi.org/10.1007/s10854-022-08148-2

2. Salih, E. Y., Ali Bashir, M. B., Rajpar, A. H., & Badruddin, I. A. (2022). Fabrication and characterization of porous Si/CuO film for visible light MSM photodetector: The effect of post-processing temperature. Ceramics International, 48(7), 9965–9972. https://doi.org/10.1016/j.ceramint.2021.12.203

3. Alfaro Cruz, M. R., Sanchez-Martinez, D., & Torres-Martínez, L. M. (2020). CuO thin films deposited by DC sputtering and their photocatalytic performance under simulated sunlight. Materials Research Bulletin, 122, 110678. https://doi.org/10.1016/j.materresbull.2019.110678

4. Al-Kuhaili, M. F. (2008). Characterization of copper oxide thin films deposited by the thermal evaporation of cuprous oxide (Cu2O). Vacuum, 82(6), 623–629. https://doi.org/10.1016/j.vacuum.2007.10.004

5. Mahana, D., Mauraya, A. K., Singh, P., & Muthusamy, S. K. (2023). Evolution of CuO thin films through thermal oxidation of Cu films prepared by physical vapour deposition techniques. Solid State Communications, 366–367, 115152. https://doi.org/10.1016/j.ssc.2023.115152

6. Zhong, Y., Dou, Z., Wang, R.-F., Lv, Y.-F., Han, S., Yan, H., … Xue, Q.-K. (2021). Real-space characterization of tetragonal CuO epitaxial films. Applied Physics Letters, 119(17), 172602. https://doi.org/10.1063/5.0069356

7. Welegergs, G. G., Mehabaw, Z. ., Gebretinsae, H. G., Tsegay, M. G., Kotsedi, L., Khumalo, Z., … Maaza, M. (2023). Electrodeposition of nanostructured copper oxide (CuO) coatings as spectrally solar selective absorber: Structural, optical and electrical properties. Infrared Physics & Technology, 133, 104820. https://doi.org/10.1016/j.infrared.2023.104820

8. Panda, R., Patel, M., Thomas, J., & Joshi, H. C. (2022). Pulsed laser deposited Cu2O/CuO films as efficient photocatalyst. Thin Solid Films, 744, 139080. https://doi.org/10.1016/j.tsf.2022.139080

9. Hassen, M. J., Seno, N. I., Alalousi, M. A., & Rzaij, J. M. (2024). Effect of copper content on the structural properties of the CuxCo1-XFe2O4 Nanostructured Spinel Ferrite Based on Williamson-Hall Analysis Maram. Samarra Journal of Pure and Applied Science www.sjpas.com, 4(6), 208–218. https://doi.org/10.54153/sjpas.2024.v6i4.950 Article

10. Singh, R. S., Patidar, R. D., Singh, A. K., Deshmukh, K., Thakur, K., & Gautam, A. (2023). Simple Thermal Annealing-Assisted Direct Synthesis and Optical Property Study of CuO Nanoparticles Incorporated Polyvinyl Alcohol Films. physica status solidi (a), 220(17),

2300328. https://doi.org/10.1002/pssa.202300328

11. Sayyed, S. G., Shaikh, A. V., Shinde, U. P., Hiremath, P., & Naik, N. (2023). Copper oxide-based high-performance symmetric flexible supercapacitor: potentiodynamic deposition. Journal of Materials Science: Materials in Electronics, 34(17), 1361. https://doi.org/10.1007/s10854-023-10738-7

12. Yang, Y., Gao, L., Han, Y., Gao, Q., Lan, R., & Shen, Y. (2024). Passively Q-switched Tm:YAP laser based on WSe2/CuO heterojunction saturable absorber. Applied Physics B, 130(10), 171. https://doi.org/10.1007/s00340-024-08311-z

13. Mohammed Enad, A., & Rzaij, J. M. (2024). Synthesis of CuO Thin Film Incorporated with Nanostructured Nd 2 O 3 Deposited by Pulsed Laser Deposition for Ammonia Sensing Applications. Nano. https://doi.org/10.1142/S1793292024501133

14. Rzaij, J. M. (2023). A novel room-temperature nitrogen dioxide gas sensor based on silver-doped cerium oxide thin film. Sensors and Actuators A: Physical, 363, 114748. https://doi.org/10.1016/j.sna.2023.114748

15. Chen, X., Ren, F., Gu, S., & Ye, J. (2019). Review of gallium-oxide-based solar-blind ultraviolet photodetectors. Photonics Research, 7(4), 381. https://doi.org/10.1364/PRJ.7.000381

16. Enad, A. M., & Rzaij, J. M. (2024). Investigate the structural , morphological , and topographical characteristics of CuO thin films utilizing a pulsed laser deposition method. Journal of Theoretical and Applied Physics, 18(AICIS'23), 1–8. https://doi.org/10.57647/j.jtap.2024.si-AICIS23.03

17. Klimov, V. I. (2007). Spectral and Dynamical Properties of Multiexcitons in Semiconductor Nanocrystals. Annual Review of Physical Chemistry, 58(1), 635–673. https://doi.org/10.1146/annurev.physchem.58.032806.104537

18. Tawfeeq, H. A., & Rzaij, J. M. (2024). The effect of Nb2O5 and pdo nanostructures coating on the structural and morphological properties of CdO thin films. In 4TH INTERNATIONAL CONFERENCE ON PURE SCIENCES: ICPS2023 (p. 050011). Baghdad, Iraq. https://doi.org/10.1063/5.0196260

19. Tejani, J., Shah, R., Vaghela, H., Vajapara, S., & Pathan, A. (2020). Controlled Synthesis and Characterization of Lanthanum Nanorods. International Journal of Thin Films Science and Technology, 9(2), 119–125. https://doi.org/10.18576/ijtfst/090205

20. Shawki, O. S., & Rzaij, J. M. (2023). Effect of Fe2O3 upper layer on structural, morphological, and photoluminescence characteristics of TiO2 thin film prepared by chemical spray pyrolysis. In 1st Diyala International Conference for Pure and Applied Science (ICPAS2021) (p. 020009). Iraq: AIP Conference Proceedings. https://doi.org/10.1063/5.0112172

21. Ramadhan, A. A., Hameed, M. M., Salman, M. O., & Nasir, E. M. (2024). Enhanced Gas Sensing Performance of Plasma-Treated Tin-Zinc–Oxide Thin Films Deposited by Spray Pyrolysis. Iraqi Journal of Applied Physics, 20(3), 485–492.

22. Dathan, M. J., Hassan, B. F., Abduljabbarb, Q. A., & Rzaij, J. M. (2023). Nickel oxide doping impact on the NO2 sensing properties of nanostructured zinc oxide deposited by spray pyrolysis. Digest Journal of Nanomaterials and Biostructures, 18(4), 1159–1167. https://doi.org/10.15251/DJNB.2023.184.1159

23. Farhad, S. F. U., Webster, R. F., & Cherns, D. (2018). Electron microscopy and diffraction studies of pulsed laser deposited cuprous oxide thin films grown at low substrate temperatures. Materialia, 3, 230–238. https://doi.org/10.1016/j.mtla.2018.08.032

24. Anitha, M., Anitha, N., Saravanakumar, K., Kulandaisamy, I., & Amalraj, L. (2018). Effect of Zn doping on structural, morphological, optical and electrical properties of nebulized spray-deposited CdO thin films. Applied Physics A: Materials Science and Processing, 124(8), 0. https://doi.org/10.1007/s00339-018-1993-7

25. Gnanasekar, T., Valanarasu, S., Ubaidullah, M., Alam, M., Nafady, A., Mohanraj, P., … Pandit, B. (2022). Fabrication of Er, Tb doped CuO thin films using nebulizer spray pyrolysis technique for photosensing applications. Optical Materials, 123, 111954. https://doi.org/10.1016/j.optmat.2021.111954

26. Abdo, S. K., & Rzaij, J. M. (2021). Copper Molarity Effect on the Optical Properties of Cu2CdSnS4 Quaternary Thin Films. Iraqi Journal of Science, 62(5), 1513–1523. https://doi.org/10.24996/ijs.2021.62.5.15

27. Modhi, M. K., & Rzaij, J. M. (2023). Synthesis and characterization study of CuO thin film and CuO-CeO2 nanostructured composite using chemical spray pyrolysis. In AL-KADHUM 2ND INTERNATIONAL CONFERENCE ON MODERN APPLICATIONS OF INFORMATION AND COMMUNICATION TECHNOLOGY (p. 030066). Baghdad, Iraq: AIP Conference Proceedings. https://doi.org/10.1063/5.0120468

28. Basith, N. M., Vijaya, J. J., Kennedy, L. J., & Bououdina, M. (2014). Structural, morphological, optical, and magnetic properties of Ni-doped CuO nanostructures prepared by a rapid microwave combustion method. Materials Science in Semiconductor Processing, 17, 110–118. https://doi.org/10.1016/j.mssp.2013.09.013

29. Ong, C. H., & Gong, H. (2003). Effects of aluminum on the properties of p-type Cu–Al–O transparent oxide semiconductor prepared by reactive co-sputtering. Thin Solid Films, 445(2), 299–303. https://doi.org/10.1016/S0040-6090(03)01175-1

IRAQI Academic Scientific Journals
Samarra Journal of Pure and Applied Science
SJPAS
مجلة سامراء للعلوم الصرفة والتطبيقية
www.sjpas.com
p ISSN: 2663-7405
e ISSN: 2789-6838

دراسة الخصائص التركيبية والبصرية لأغشية أكسيد النحاس الرقيقة الممزوجة بأكسيد اللانثانيوم المترسبة باستخدام الترسيب بالليزر النبضي لتطبيقات الأجهزة الالكتروبصرية وأجهزة استشعار الغاز المستقبلية

عبير محمد عناد، جمال مال الله رزيج*
قسم الفيزياء، كلية العلوم، جامعة الأنبار، الرمادي، العراق

معلومات البحث:
تاريخ الاستلام: 2025/01/15
تاريخ التعديل: 2025/02/13
تاريخ القبـــول: 2025/03/20
تاريخ الـنشر: 2025/06/30
الكلمات المفتاحية:
أكسيد النحاس، العناصر الأرضية النادرة، PLD، La_2O_3، الإلكترونيات البصرية، مستشعر الغاز .

معلومات المؤلف
الايميل: sc.jam72al@uoanar.edu.i
رقم الهاتف:

الخلاصة:
يُظهر مزيج طلاءات أكاسيد المعادن الرقيقة مع العناصر الأرضية النادرة إمكانات كبيرة لتحسين الخصائص التركيبية والبصرية في تطوير الأجهزة البصرية الإلكترونية وأجهزة استشعار الغاز. بحثت هذه الدراسة في تأثير مزج نسب وزنية متباينة لأكسيد اللانثانيوم (La_2O_3) على الخصائص التركيبية والطوبوغرافية والتركيب المايكروي والانتقال الإلكتروني لأغشية أكسيد النحاس الرقيقة (CuO). تم فحص خصائص الأغشية المطورة عبر الترسيب بالليزر النبضي باستخدام حيود الأشعة السينية (XRD) وتقنية الأشعة السينية المشتتة للطاقة (EDX) ومجهر القوى الذرية (AFM) والمجهر الالكتروني الماسح ذو المجال الانبعاثي (FE-SEM) والتألق الضوئي (PL) وتقنية الأشعة فوق البنفسجية المرئية. وفقًا لحليل النتائج التركيبية، كان تبلور غشاء أكسيد النحاس متعدد البلورات مع ذروة مهيمنة نحو ذروة الحيود (111). انخفضت شدة الذروة السائدة مع زيادة محتوى أكسيد اللانثانيوم، وانخفض الحجم البلوري من 19 إلى 17.4 نانومتر. أكد التحليل الأولي للعناصر وجود عناصرالاوكسجين والنحاس واللانثانيوم وعدم وجود ذروات انبعاث EDX أخرى تتوافق مع عناصر أو شوائب غريبة. كان لغشاء CuO المترسب توزيع حبيبات نانوية واسع، بمتوسط حجم حبيبات 100 نانومتر ومتوسط جذر تربيعي لمعدل الخشونة 3.7 نانومتر. في المقابل، أظهرت عينات La_2O_3 الممزوجة مع CuO انخفاضًا في متوسط حجم الحبيبات وزيادة ومتوسط الجذر التربيعي لمعدل الخشونة إلى 4.9 نانومتر لأكبر نسبة خلط من La_2O_3. أكد التحليل البصري انخفاض في طيف امتصاص CuO وتحول أزرق في حافة الامتصاص مع زيادة نسبة خلط La_2O_3، مما رفع مقدار فجوة الطاقة البصرية من 2.25 إلكترون فولت إلى 2.85 إلكترون فولت. تشير النتائج إلى أن خلط La_2O_3 يعدل بشكل كبير الخصائص البنيوية والبصرية لأغشية CuO الرقيقة، مما يجعل الأغشية المطورة مرشحة مناسبة لاستشعار الغاز والتطبيقات البصرية الإلكترونية..